Journal of Molecular Liquids 307 (2020) 112954

Contents lists available at ScienceDirect

Journal of Molecular Liquids

journal homepage: www.elsevier.com/locate/molliq

The inhibitory effect of citrus flavonoids naringenin and hesperetin against purine nucleoside phosphorylase: Spectroscopic, atomic force microscopy and molecular modeling studies

Xingang Lv [a], Qilei Wang [a], Lang-Hong Wang [a,*], Er-Fang Ren [b], Deming Gong [c]

[a] College of Food Science and Technology, Northwest University, Xi'an 710069, China
[b] Guangxi Subtropical Crops Research Institute, Nanning 530001, China
[c] Department of Biomedicine, New Zealand Institute of Natural Medicine Research, Auckland 2104, New Zealand

ARTICLE INFO

Article history:
Received 3 March 2020
Accepted 20 March 2020
Available online 21 March 2020

Keywords:
Citrus flavonoid
Purine nucleoside phosphorylase
Enzymatic kinetics
Molecular modeling
Atomic force microscopy

ABSTRACT

In this work, the inhibitory effect of two citrus flavonoids naringenin and hesperetin on human purine nucleoside phosphorylase (hPNP) and their binding mechanism were evaluated. Results from enzymatic kinetics revealed that naringenin and hesperetin reversibly inhibited hPNP via a mixed-type manner with IC_{50} values of 4.83×10^{-4} M and 5.32×10^{-4} M, respectively. Analysis of molecular modeling revealed that both naringenin and hesperetin bound directly into the active site by generating multiple forces including hydrogen bonding, π–π and π-Alkyl interactions with His64, Glu201, Ser220, His257, Phe200 and Val217 residues of hPNP, which caused the inhibition of hPNP activity. Moreover, conformational analysis by three-dimension fluorescence, circular dichroism and atomic force microscopy revealed that the binding of naringenin and hesperetin to hPNP induced changes in the microenvironment, secondary structure and morphology of hPNP. These results suggested that occupying the active site and enzymatic conformational perturbation induced by naringenin and hesperetin are the main reasons for reducing the inhibition of hPNP activity, which would be helpful in understanding the inhibitory mechanism of naringenin and hesperetin against hPNP.

1. Introduction

Purine nucleoside phosphorylase (PNP) is a crucial enzyme in the metabolism of purines with reversible phosphorolysis of guanine, hypoxanthine, and many of nucleoside analogues [1]. Structural analysis has revealed that PNPs found in mammals are homotrimers that specific to cleave the glycosidic bond of 6-oxopurine nucleosides while that from prokaryotes are homohexamers vary in their specificity, accepting 6-amino purine nucleosides as well [2]. PNP allows the cells to form nucleotides by using purine bases, to avoid the energy-wasting ex-novo synthesis. Therefore, it is essential for cell survival and function, and being involved in various diseases under abnormal activity. In humans, the deficiency of PNP leads to T-lymphocytopenia, a kind of metabolic disorder having immunodeficiency and depletion of T-cells [3]. However, the increase of expression levels of PNP mRNA and biological activity was found to have a relationship with T-cell cancers and in autoimmune diseases. For example, higher PNP activity was found with different types of tumors, including pancreatic ductal adenocarcinoma, human colon carcinoma, leukemias and lymphomas [4–6]. These findings suggest that PNP could be a potential therapeutic target and consequently becoming of interest in molecular biology and clinical medicine. Currently, there are only two oral PNP inhibitors (forodesine hydrochloride and ulodesine) in clinical trials for the treatment of T-cell malignancies [7]. However, these inhibitors impose efficacy and side effects with high price and complex production technology, and consequently, new inhibitors with high efficiency and minor side effects are certainly warranted.

Flavonoids, a group of bioactive substances naturally occur in various vegetables and fruits having a broad range of pharmaceutical activities [8–10]. Naringenin (NAR, Fig. 1A) and hesperetin (HES, Fig. 1B) are two of major bioactive flavonoids in grapefruit and sweet orange, respectively. They have been well acclaimed for antioxidant, anti-inflammatory, anti-ulcer and anti-carcinogenic activity, which are presumed to beneficial for reducing the risk of cardiovascular disease and cancers. Moreover, NAR and HES are regarded to have the potency in inhibiting a variety of enzymes that play crucial roles in promoting human health and regulating physiological functions. For example, a report conducted by Priscilla et al., suggesting NAR is an effective inhibitor of intestinal α-glucosidase to reduce the postprandial blood glucose levels [11]. Luigi and coworkers found that HES is of potential clinical relevance that inhibits the activity of cytochrome P450 (CPY2C9) at low micromolar concentrations [12]. Moreover, both NAR and HES also have been revealed to have abilities

* Corresponding author.
E-mail address: wlhong@nwu.edu.cn (L.-H. Wang).

https://doi.org/10.1016/j.molliq.2020.112954
0167-7322/

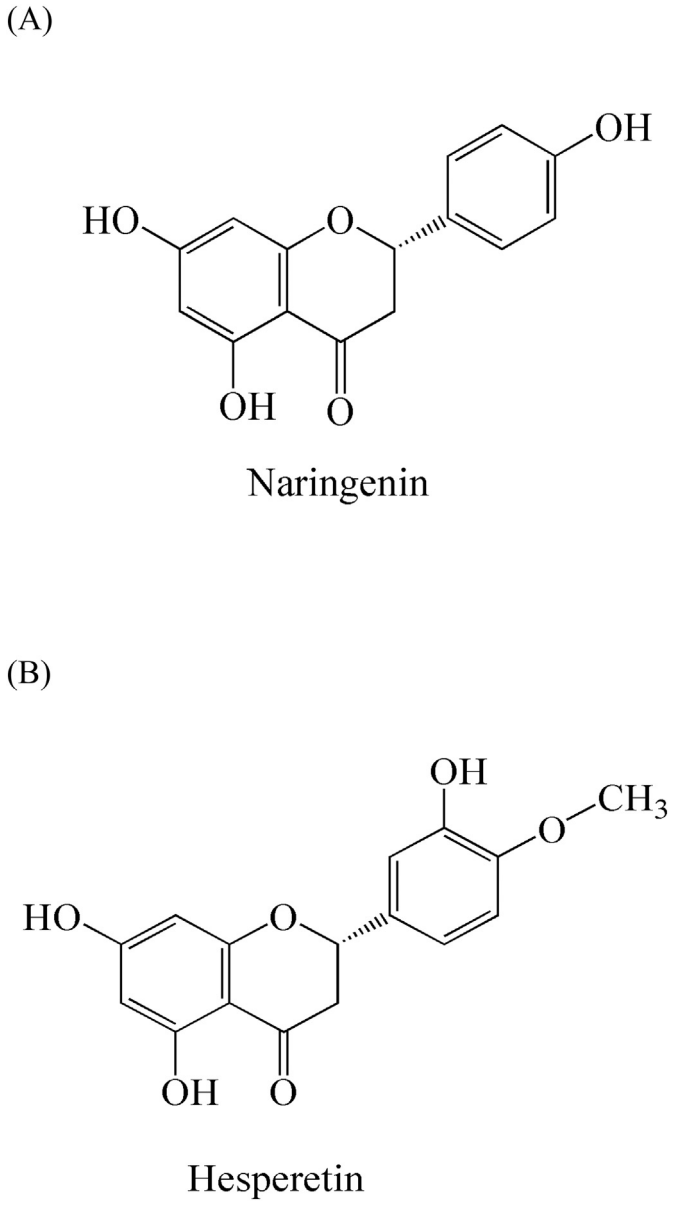

Fig. 1. The molecular structure of NAR (A) and HES (B).

in inhibiting tyrosine kinase activity in vitro by occupying the ATP binding site of the enzyme [13]. However, no information is available about their inhibitory activity against hPNP. Since hPNP is considered as a therapeutic target for the therapy of T-cell cancers and in autoimmune diseases, finding safe and high-effective hPNP inhibitors can help to extend different ways for the treatment of these diseases.

Therefore, in this work, the inhibitory effects of NAR and HES on hPNP and their interactions including binding constant, site and hPNP conformational changes were investigated by high-performance liquid chromatography (HPLC), fluorescence and 3D-fluorescence, circular dichroism (CD), atomic force microscopy (AFM), and computational molecular dockings. This study was expected to provide useful information for potential applications of NAR and HES as hPNP inhibitors in the clinic.

2. Materials and methods

2.1. Reagents

Human purine nucleoside phosphorylase (hPNP, EC 2.4.2.1, 303.2 U mL^{-1}) and inosine (purity ≥99%) were from Sigma–Aldrich Co. (St. Louis, MO, USA). Stock solutions of hPNP (2.60×10^{-4} M) and inosine (2.84×10^{-2} M) were prepared in buffered aqueous solution (0.01 M potassium phosphate buffer with 1 mM $MgCl_2$, pH 7.4). NAR (purity, 99.0%) and HES (purity, 99.0%) were purchased from Aladdin Chemical Co. (Shanghai, China), and their stock solution (1.5×10^{-2} M) were prepared in dimethylsulfoxide (DMSO) under sterile conditions which was then stored in the dark at 4 °C. The final concentrations of DMSO in the experiments were kept at <2.0%, which shows no effect on the structure and activity of the enzyme. All stock solutions were stored at 0–4 °C. All chemicals were of analytical reagent grade. Ultrapure water was used in the preparation of the samples and throughout the whole experiment.

2.2. hPNP activity and type inhibition analysis

The activity of hPNP was determined the phosphorolysis of inosine to hypoxanthine based on a published method [2]. Briefly, 1.0 mL hPNP (1.30×10^{-7} M) was incubated with varying concentrations of NAR/HES in potassium phosphate buffer solution for 3 h at 37 °C with gentle mixing. Then, the catalytic reaction was initiated by adding inosine (final concentration was 1.42×10^{-4} M). After 1 min, the reaction was stopped by heating the mixture in boiling water (100 °C) for 3 min to completely extinguish catalytic activity. After denatured enzymes were removed by centrifugation (15,000 ×*g*, 10 min), aliquots of 500 μL of the supernatants were filtered using 0.22 μm syringe filters and collected for liquid chromatography. The determination of hypoxanthine was carried out by loading 20 μL each sample on an XSelect®-HSS T3 (4.6 × 250 mm, 5 μm, Waters, Milford, MA, USA) with the absorbance detection at 254 nm. The C18 column (column temperature, 30 °C) was used with 10 mM ammonium formate (pH 3.6) as the mobile phase in the flow rate of 1 mL/min.

The relative enzymatic activity was expressed as *E* (%), based on the Eq. (1):

$$E(\%) = C_1/C_0 \times 100\% \quad (1)$$

where E, C_1 and C_0 represent the relative activity of hPNP, the concentration of hypoxanthine in the absence and presence of flavonoids (NAR or HES), respectively.

In order to characterize the kinetic mechanism of inhibition of hPNP by NAR and HES, the formation of hypoxanthine was catalyzed by hPNP was measured in the above-specified incubation mixture containing increasing concentrations of inosine in the absence or presence of four concentrations of NAR or HES (0, 1.25, 2.50, 3.7×10^{-4} M). Based on the experiment above, the constant of inhibition (*K*m) and the inhibitory type could be determined by the Lineweaver—Burk plot.

2.3. Fluorescence studies

The fluorescence spectra of hPNP in the presence of different amounts of NAR/HES were performed under 37 °C using a model F-7000 fluorescence spectrophotometer (Hitachi High-Technologies Co., Tokyo, Japan) with an excitation wavelength of 280 nm. Both the excitation and emission bandwidths were set at 5.0 nm. Appropriate blanks corresponding to the buffer were subtracted to correct background fluorescence, and the inner filter effects according to a previous method [14].

The three-dimensional fluorescence spectra of hPNP in the absence and presence of NAR/HES were recorded at excitation and emission wavelengths from 200 to 450 nm using 5.0/5.0 nm slit widths.

2.4. Circular dichroism (CD) studies

The CD signal of hPNP was recorded in a BioLogic MOS 450 CD spectrometer (Bio-Logic, Claix, France) using a 0.1 cm path length cuvette and baseline corrected for the buffer signal. The concentration of hPNP

was kept at 5.4 μM, and the molar ratios of the mixture ([NAR or HES]/[hPNP]) were varied as 0:1, 2:1 and 4:1.

2.5. Molecular simulation

Molecular docking of the optimized ligands (NAR and HES) with hPNP (PDB: 3K8O) was performed in AutoDockTools-1.5.6rc3 with Autodock 4.2 program package using Lamarckian genetic algorithm (LGA) as the search engine. The default grid spacing of 0.7 Å with a grid-box 120 Å × 120 Å × 120 Å was applied by AutoGrid program. For each ligand, 100 possible conformations were generated, and based on glide score and conformation clusters, the optimal conformation with the lowest energy was selected for further analysis.

2.6. Atomic force microscopy (AFM) measurements

AFM measurements were performed using an MFP-3D-S AFM (Santa Barbara, CA) in tapping mode as described previously [15]. Briefly, 1.0 mL hPNP (1.30×10^{-7} M) with NAR/HES (molar ratio, 1:0 and 1:5) was incubated for 3.0 h at 25 °C. Then, 15 μL of each sample was air dried on a freshly cleaved mica plate with standing for 0.5 h, and followed by washed gently with 300 μL ultrapure water. After suitable drying and calibration, the desired AFM images were obtained.

2.7. Statistical analysis

Results were expressed as means ± SD. Data were analyzed using OriginPro 8.0 (OriginLab, Northampton, MA, USA).

3. Results and discussion

3.1. The inhibitory effects on hPNP

Fig. 2A and B exhibit the effects of NAR and HES in the range of concentrations from 0 to 6.88×10^{-4} M on the hypoxanthine formation, respectively. Obviously, the production of hypoxanthine was gradually decreased with the increasing concentration of NAR and HES, indicating that both they decreased hypoxanthine formation in a concentration-dependent manner. These results were well consistent with the loss relative activity of hPNP (Fig. 2C). The concentration of NAR and HES that resulted in a loss of 50% enzyme activity (IC_{50}) was estimated to be 4.83×10^{-4} M and 5.32×10^{-4} M, respectively, implying that NAR and HES might have a potential to inhibit the activity of hPNP.

3.2. Inhibition mechanism of NAR and HES on the activity of hPNP

To confirm the reversibility of these two citrus flavonoids inhibition toward hPNP, the plots of the v vs [hPNP] (enzyme concentration) in the presence of increasing concentrations of NAR and HES were constructed. As shown in Fig. 3A and B, all data were fitted and gave a family of straight lines with intercepts essentially equal to 0. Moreover, increasing concentrations of NAR and HES led to a decrease in the slopes of the lines, suggesting that these two flavonoids reversibly inhibited hPNP activity, that led to the decrease of efficiency in term of the production of hypoxanthine [16].

The kinetic behavior of hPNP during phosphorolysis of inosine in the presence of NAR and HES was evaluated using double-reciprocal Lineweaver-Burk plots at different concentrations of inosine and NAR/HES. As can be seen in Fig. 3C and D, the Lineweaver-Burk plots gave a family of lines with different slopes and different Y-axis intercepts indicating that NAR and HES are typically mixed-type hPNP inhibitors [17,18]. This means that NAR and HES not only bind with the free hPNP but also with the inosine–hPNP complex resulting in an increase of K_m and a decrease of V_{max}.

Based on the Michaelis−Menten kinetics, the Lineweaver-Burk equation for mixed type inhibition is as follows [19]:

$$\frac{1}{v} = \frac{K_m}{V_{max}}\frac{1}{[S]}\left(1 + \frac{[I]}{K_i}\right) + \frac{1}{V_{max}}\left(1 + \frac{[I]}{K_{is}}\right) \quad (2)$$

Secondary plots can be built as:

$$\text{Slop} = \frac{K_m[I]}{V_{max}}K_i + \frac{K_m}{V_{max}} \quad (3)$$

$$\text{Y-intercept} = \frac{1}{V_{max}^{app}} = \frac{1}{V_{max}} + \frac{1}{K_{is}V_{max}}[I] \quad (4)$$

where v is the enzyme reaction rate in the absence and presence of NAR or HES. K_m is the Michaelis–Menten constant. [I] is the concentration of NAR or HES, and [S] is the concentration of inosine; K_i and K_{is} are the equilibrium constant for binding with free enzyme and the enzyme-substrate complex, respectively.

The secondary plot of slope or Y-intercept vs. [NAR] was linear (Fig. 3C and D inset), suggesting that NAR and HES had a single inhibition site or a single class of inhibition sites on hPNP [20]. Based on secondary plots, the values of K_i for NAR and HES were obtained to be $(3.48 \pm 0.1) \times 10^{-4}\ M^{-1}$ and $(3.94 \pm 0.1) \times 10^{-4}\ M^{-1}$, respectively. Accordingly, the K_{is} of inhibitors with respect to inosine–hPNP complexes of NAR and HES were determined to be $(1.53 \pm 0.3) \times 10^{-3}\ M^{-1}$ and $(1.27 \pm 0.3) \times 10^{-3}\ M^{-1}$. The value of K_{is} was obviously greater than that of K_i, indicating that the affinity of NAR and HES to hPNP may be stronger than that of the inosine–hPNP complex [21]. Similar results were reported by Wen and coworkers, who also observed that flavonoids including chrysin, baicalein and apigenin performed as mixed-type inhibitors of hPNP [2].

3.3. Fluorescence quenching of hPNP by Nar and HES

The inhibitory activity of NAR and HES on hPNP demonstrates that there is a direct interaction between these two flavonoids and hPNP. Therefore, fluorescence quenching of hPNP was induced by NAR and HES to investigate their interactions. As shown in Fig. 4A and B, the maximum fluorescence emission peak of hPNP at 338 nm decreased with an apparent red-shift after gradually adding of NAR and HES (0 to 5.73×10^{-4} M), indicating that the binding of NAR and HES to hPNP indeed happened, and their interactions resulted in some perturbations in the conformation of hPNP [22].

For fluorescence quenching, an improved method was used to calculate the binding constant (K_a) and the number of binding sites (n) [23].

$$\log\frac{F_0 - F}{F} = n\ \log K_a - n\ \log\frac{1}{[Q_t] - \frac{F_0 - F}{F}[P_t]} \quad (5)$$

where [P_t] and [Q_t] denote the total concentrations of the hPNP and NAR/HES, respectively. F_0 and F are the corrected fluorescence intensities of hPNP in the absence and presence of NAR/HES, respectively, based on a reported method [24]. Based on the Eq. (5) and Fig. 4C, the calculated K_a and n values for NAR−hPNP and HES−hPNP were $(4.73 \pm 0.03) \times 10^4\ M^{-1}$ and $(3.94 \pm 0.04) \times 10^4\ M^{-1}$, and 1.25 and 1.36, indicating a strong static interaction of these two flavonoids with hPNP [25]. The estimated K_a values for NAR−hPNP was larger than HES−hPNP, suggesting that the stability of NAR–hPNP > HES–hPNP, which is well consistent with the K_i values from inhibition kinetic results.

3.4. Three-dimensional fluorescence analysis

To study the possible hPNP conformational change, 3-D fluorescence spectra of hPNP and the NAR/HES−hPNP complex were measured,

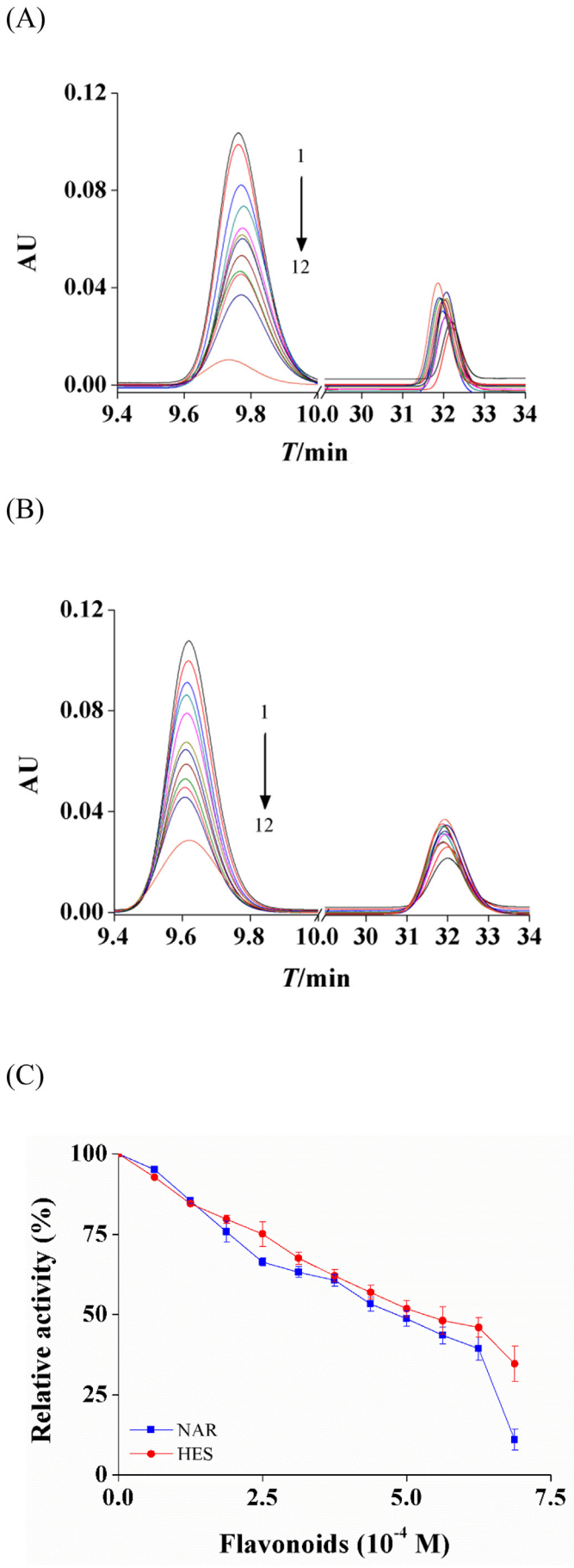

respectively. As shown in Fig. 5A, Peak 1 ($\lambda_{ex} = 280$ nm, $\lambda_{em} = 335$ nm) mainly reflects the spectral behavior of Trp and Tyr, which is mainly caused by the transition of $n \rightarrow \pi^*$ of aromatic amino acids in hPNP, and Peak 2 ($\lambda_{ex} = 230$ nm, $\lambda_{em} = 335$ nm) exhibits the fluorescence properties of polypeptide backbone structure of hPNP [26]. A direct comparison of Fig. 5A with B and C clearly reveal the 3D fluorescence characteristics of hPNP as a result of interaction with NAR and HES in terms of emission intensity reduction and position of both peak 1 and peak 2. Specifically, the fluorescence intensity of Peak 1 was decreased from 2363 to 815 and 1026 with the addition of NAR and HES, while Peak 2 was decreased from 1085 to 86.1 and 103, respectively. Moreover, both Peak 1 and 2 have an apparent red-shift in that λ_{em} at 335 nm moved to 350 nm. Since the two peaks in hPNP originate from different types of residues, these perturbations suggested the microenvironment of tryptophan residues and conformation of the binding of NAR and HES to hPNP induced some conformational and microenvironmental changes [27,28].

3.5. CD spectra analysis

CD spectroscopy is a practical and sensitive in analyzing the conformation (secondary and tertiary structure) changes of proteins [29]. Generally, CD spectra of proteins could be divided into two wavelength regions, namely far-UV CD and near-UV CD spectrum, which located in the range of 190–250 nm and 250–350 nm, respectively. Therefore, this method was used to study the alterations in the secondary and tertiary structure of hPNP after being exposed to NAR and HES.

Fig. 6A and C shows far UV-CD measurements (190–250 nm) of free hPNP and NAR/HES–hPNP complexes that revealed the structural changes of hPNP. The free hPNP displayed a broad negative band around 210–230 nm, which is in good agreement with the CD spectra of human erythrocytic PNP in the literature [30]. After binding with NAR, the negative ellipticities of hPNP were decreased, indicating the noticeable change in the secondary structures induced by the binding of NAR. The relative content (%) of the secondary structure, including α-helix, β-sheet, β-turns and random coils was calculated by the DichroWeb online program (http://dichroweb.cryst.bbk.ac.uk), and listed in Table 1. This table clearly shows that the percentage of the α-helix and β-turn in the presence of certain concentrations of NAR was decreased, while β-sheet was increased. Specially, the contents of the α-helix and β-turn decreased from 26.5 to 25.0, 21.6% and from 21.1 to 19.4, 20.0%, respectively, while the contents of the β-sheet increased from 18.1 to 20.3, 23.7% at the increasing molar ratios ([hPNP/NAR]) from 1:0 to 1:2 and 1:4. Similarly, the β-sheet increased to 20.6% and 24.3%, while the α-helix reduced to 24.3% and 20.9% as well as the β-turn mildly decreased to 20.2% and 19.8% that were observed after binding with HES at molar ratios of 1:2 and 1:4. These results implied the structural compactness of hPNP, which might lead to the contraction of the hydrophobic pocket along with decreasing the landing of the substrate and finally causing an inhibition against hPNP.

The near-UV CD spectra in the region of 250–350 nm was attributed to the existence of aromatic residues (Phe, Tyr, and Trp) and disulfide bonds, which could be used to investigate the tertiary structural changes of hPNP [31,32]. With the gradual addition of NAR or HES to hPNP solution, a significant increase in the molar ellipticity was observed in the wavelength range of 280–350 nm (Fig. 6B and D), indicating alterations of the environments of Trp residues, which related to the drastic perturbations in the tertiary structure of hPNP after binding with

Fig. 2. Effects of various concentrations of NAR (A) or HES (B) on the production of hypoxanthine by hPNP. The concentration of inosine was 1.42×10^{-4} M; (C) Effect of NAR and HES on the relative activity of hPNP; the concentration of NAR/HES was 0, 0.63, 1.25, 1.88, 2.50, 3.13, …, 6.25 and 6.88×10^{-4} M for curves 1 → 12. Data are presented as the means ($n = 3$).

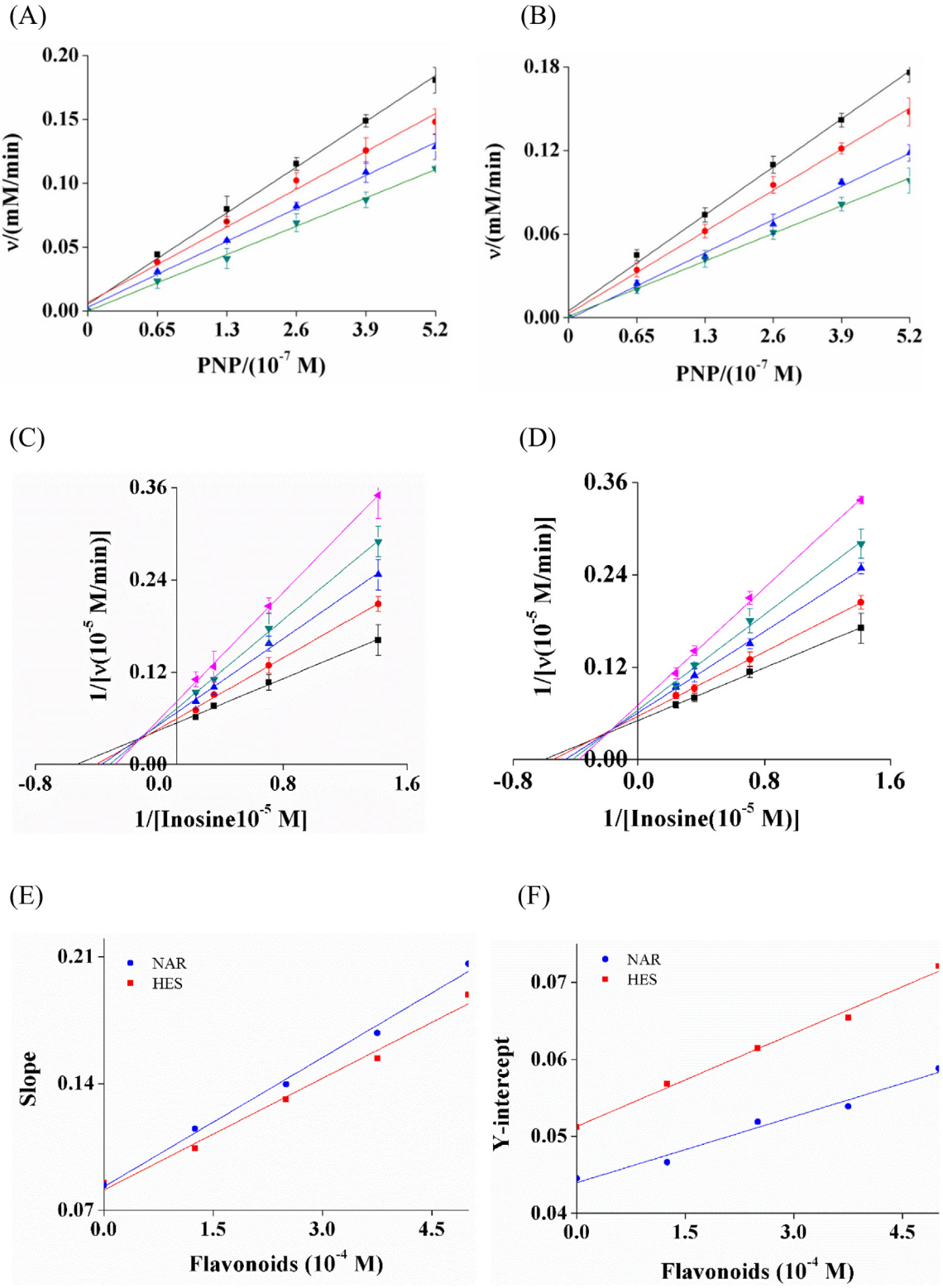

Fig. 3. Plots of v vs. [hPNP] for NAR (A) and HES (B). The concentration of NAR and HES were 0, 1.25, 2.50, 3.75 × 10^{-4} M for curves 1 → 4, respectively; the final concentration of inosine was 1.42 × 10^{-4} M and c(hPNP) = 0, 0.65, 1.30, 2.60, 3.90 and 5.20 × 10^{-7} M. (C) and (D) Lineweaver-Burk plots for NAR and HES, respectively. The final hPNP concentration was 1.30 × 10^{-7} M. The secondary plots of slope (E) and Y-intercept (F) vs. [NAR]/[HES]. NAR/HES concentrations were 0, 1.25, 2.50, 3.75 and 5.0 × 10^{-4} M for curves 1 → 5, respectively.

these two flavonoids. The above-mentioned results indicated that NAR and HES could affect the secondary structure of hPNP and result in the loss of catalytic function of hPNP, which further confirmed their inhibitory activities [33].

3.6. Surface morphological changes in hPNP

The morphological changes including distributions of shapes and size of hPNP before and after NAR/HES bound were observed by AFM

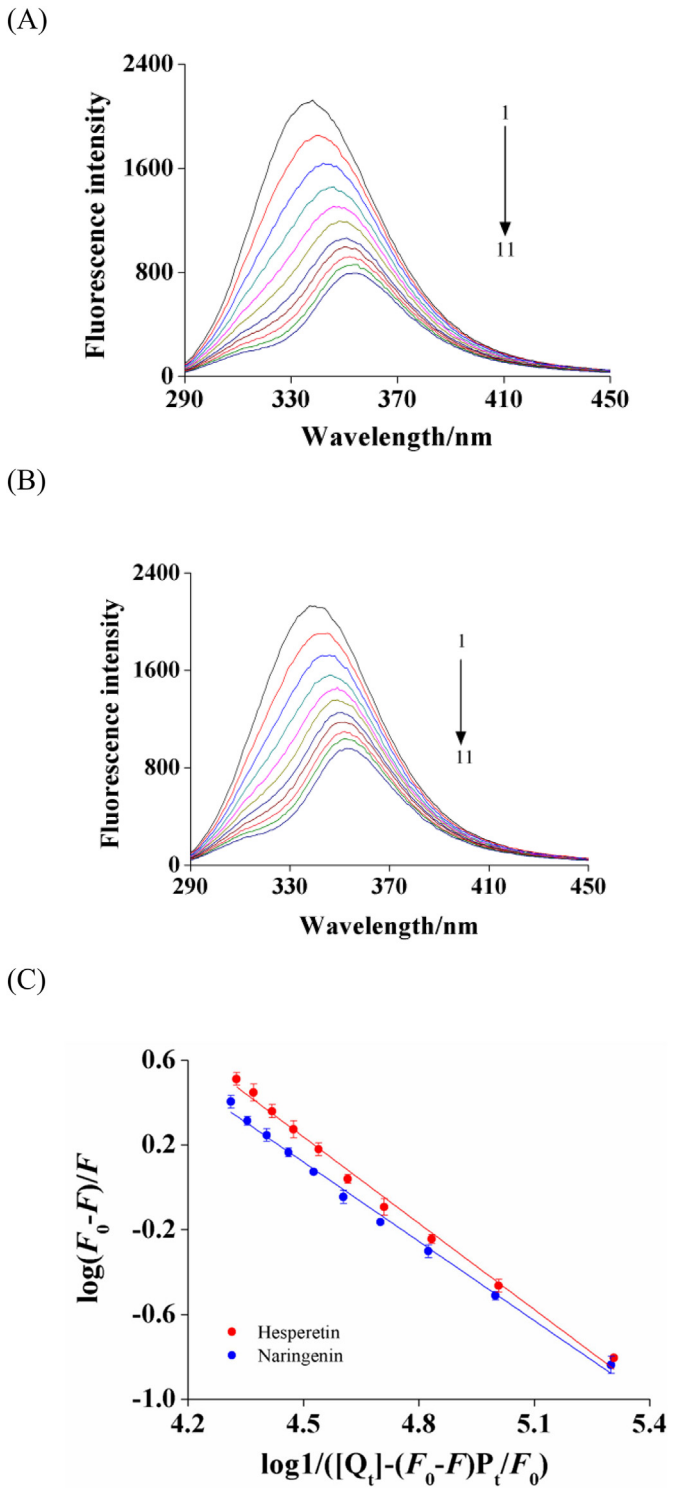

Fig. 4. The fluorescence emission spectra of PNP in the presence of increasing amounts of NAR (A) and HES (B). Fluorescence emission spectra were recorded over a wavelength range of 300–450 nm at an excitation wavelength of 280 nm. The concentrations of NAR/HES concentrations were 0, 0.52, 1.04, 1.56, 2.08, 2.61, …, 5.21 and 5.73×10^{-4} M for curves 1 → 11. The hPNP concentration was 8.67×10^{-7} M. (C) the plots for the fluorescence quenching of PNP by NAR and HES based on the Eq. (5).

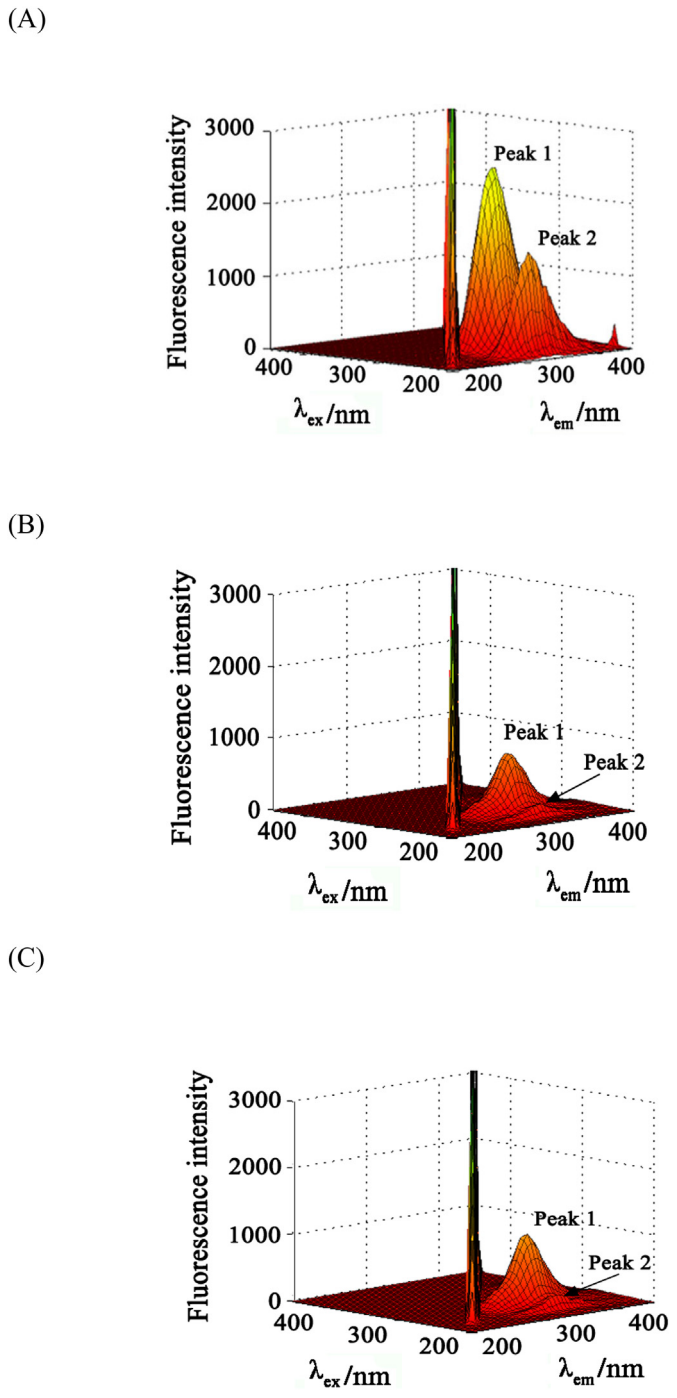

Fig. 5. (A) 3-D fluorescence spectra of hPNP (A), NAR–hPNP system (B) and HES–hPNP system (C). c(hPNP) = 8.67×10^{-7} M and c(NAR/HES) = 5.21×10^{-6} M.

(Fig. 7). Fig. 7A and B are the two- and two-dimensional topographic images of hPNP alone. The mean heights of hPNP in the absence of NAR/HES were about 3.8 nm, which well consistent with the size (3.2 nm) previously determined by Wen et al. [2]. Upon addition of NAR (Fig. 7C and D) and HES (Fig. 7E and F), the small-bright circular particles of hPNP became swollen and the mean height of hPNP reached to 12.7 and 14.2 nm, respectively. The results from AFM microscopy suggested that NAR and HES increased the hydrophobicity of hPNP surrounding microenvironment by forming a flavonoid–hPNP complex that induced both morphological changes and aggregation of hPNP molecules through protein-protein hydrophobic interaction. In this situation, the contact of hPNP molecules with water on the surface area were mostly minimized in the stable complex structures [34]. Therefore, these results obtained from AFM indicated that the formation of the NAR—hPNP or HES—hPNP complex was accompanied by a serious destabilization of the native conformation of the protein [35,36].

3.7. Computational docking of NAR and HES on hPNP

The docking analysis was performed using AutoDock 4.2 program to investigate the binding sites of NAR– and HES–hPNP interaction at a molecular level. As shown in Fig. 8A and B, the minimal binding energy of hPNP with NAR and HES were −6.8 and −6.1 kcal/mol with the highest populated clusters of 19 and 14 out of 100 (the blue bar), respectively. Based on the energetically favorable results, the lowest energies were selected to visualize the docking postures of NAR– and HES–hPNP interaction using Discovery Studio Visualizer 4.0. Results from the 2D and 3D schematic views shown that both NAR and HES docked well in the hydrophobic pocket (active site) of hPNP and surrounded by the amino acid residues, including Ser33, Val61, His64, His86, Arg84, Tyr88, Asn115, Ala116, Ala117, Gly118, Phe200, Glu201, Val217, Ser220, Met219, Asn243, Val245, His257, etc., suggesting that NAR and HES shared a common binding region with the substrate (inosine) (Fig. 8C and D). Among them, Val61, Tyr88, Ala116, Ala117, Tyr192, Val217, Met219, Val245, Val260 are hydrophobic residues, it could be speculated that the hydrophobic interactions played an important role in the binding mechanism of NAR and HES with hPNP. Moreover, the effects of hydrogen bonds, π–π (Pi-Pi) and π-Alkyl interactions could not be neglected for stabilizing NAR– and HES–hPNP postures. For NAR–hPNP interaction, NAR formed four hydrogen bonds with His64, Glu201, Ser220 and His257 of hPNP residues, and to produce π–π (Pi-Pi) and π-Alkyl forces with the amino acids Phe200, Val217 and Met219 (Fig. 8C). Similarly, in the docking of HES with hPNP, the same hydrogen bonds were found between the hydroxyl group of HES with the residues His64, Glu201, Ser220 and His257, and generate π–π (Pi-Pi) and π-Alkyl forces with Phe200 and Val217. Consequently, it can be concluded that His64, Glu201, Ser220, His257, Phe200 and Val217 around the reactive site, and played a crucial role in complexation process of NAR and HES with hPNP.

Table 1
The contents of secondary structures in hPNP in the absence and presence of NAR and HES.

Molar ratio		α-Helix	β-Sheet	β-Turn	Random coil
hPNP/NAR	1:0	26.5	18.1	21.1	34.3
	1:2	25.0	20.3	19.4	35.3
	1:4	21.6	23.7	20.0	34.7
hPNP/HES	1:0	25.6	19.0	20.5	34.9
	1:2	24.3	20.6	20.2	34.9
	1:4	20.9	24.3	19.8	35.0

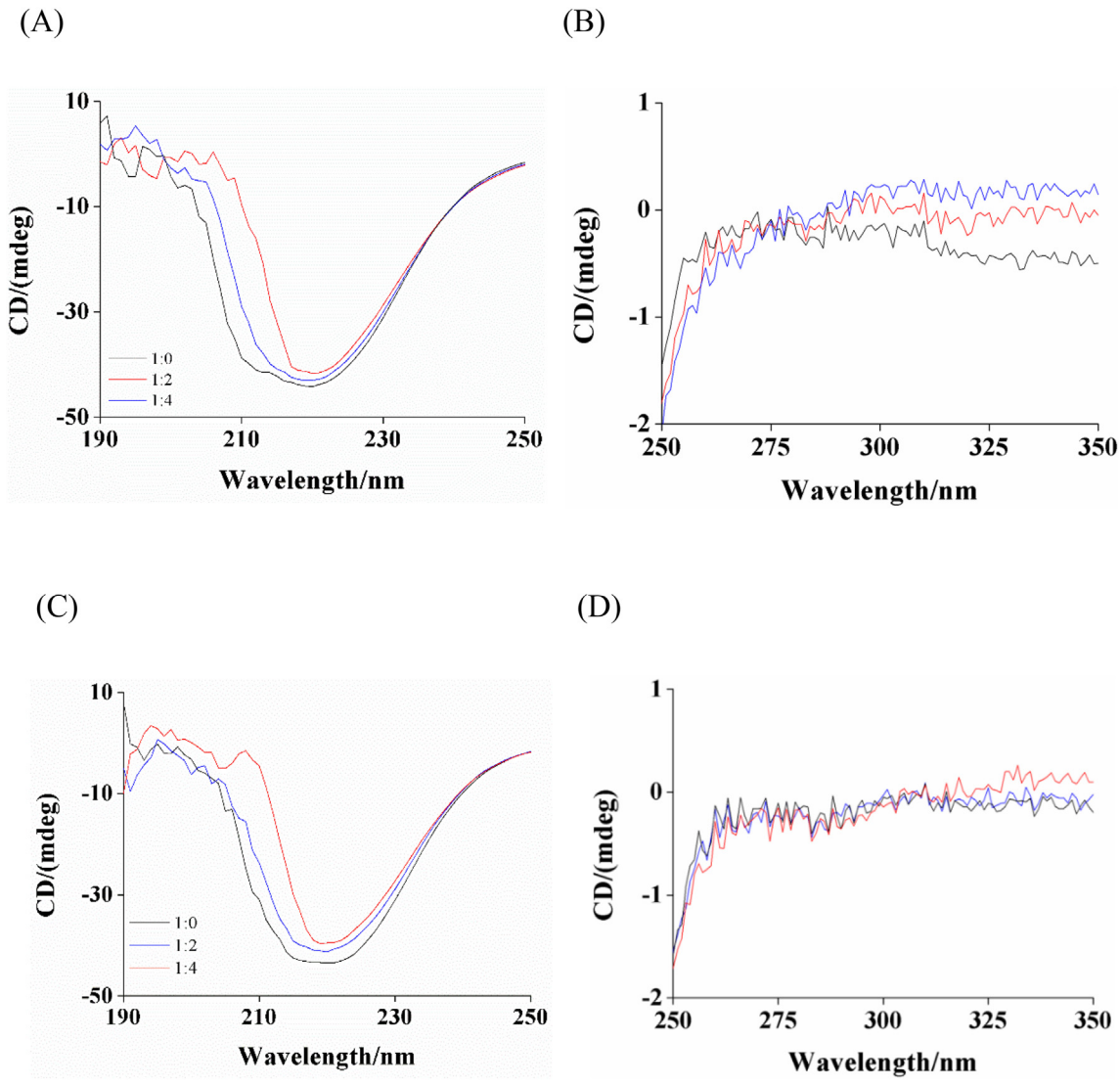

Fig. 6. The CD spectra of hPNP in the presence of increasing amounts of NAR: (A) Far-UV CD spectra and (B) Near-UV spectra; The CD spectra of hPNP in the presence of increasing amounts of HES: (C) Far-UV CD spectra and (D) Near-UV spectra; c(hPNP) = 5.4 μM, the molar ratios ([hPNP]/[Flavonoids]) are 1:0, 1:2 and 1:4, respectively.

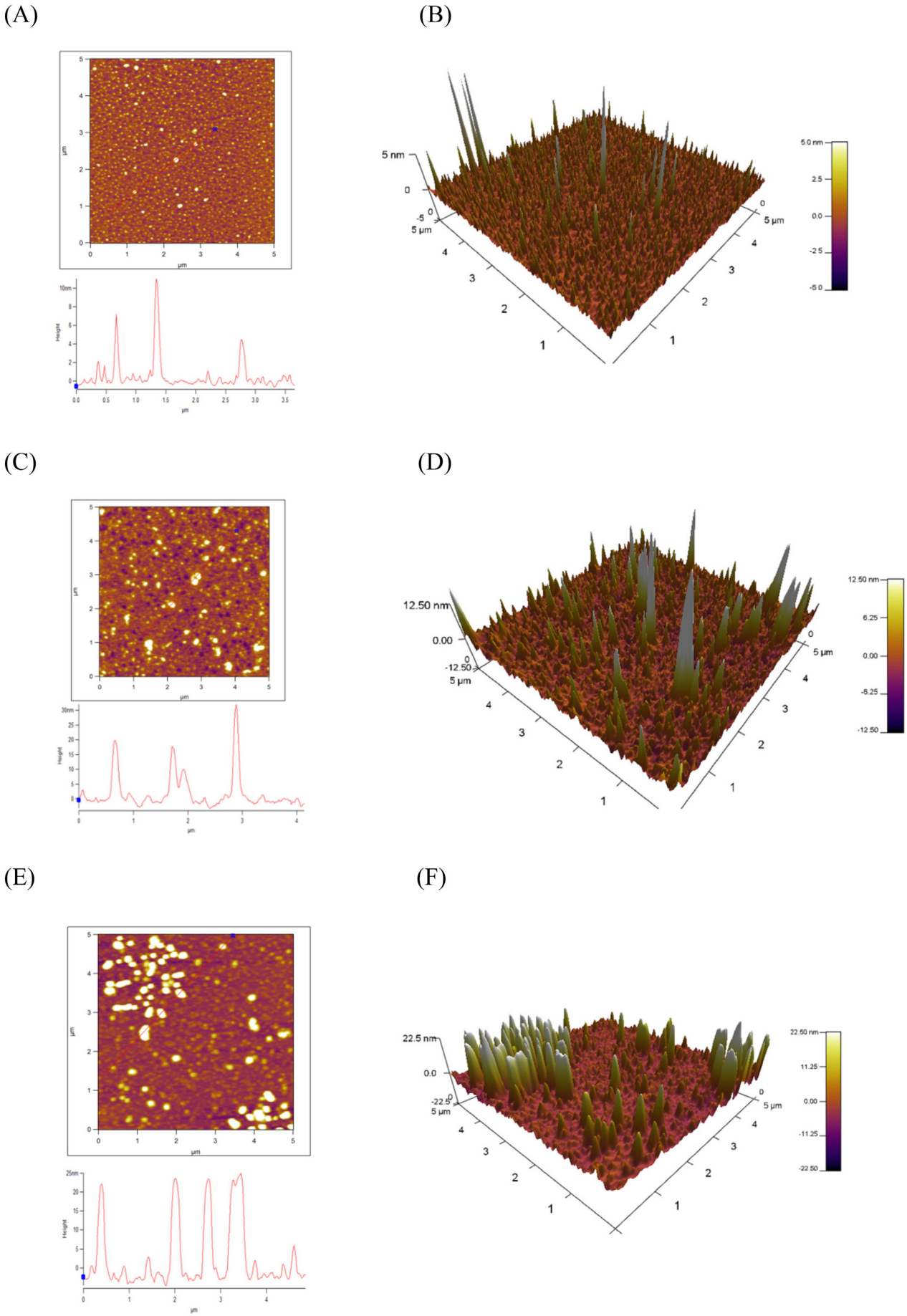

Fig. 7. AFM topography image of PNP (A), NAR–hPNP complex (C), HES–hPNP complex (E) adsorbed onto mica with tapping mode in air. The scan size of the image was 5.0 μm × 5.0 μm. *c* (PNP) = 1.30×10^{-7} mol L^{-1}, the molar ratios of flavonoids to PNP were 5:1. B, D and F are the two-dimensional graphs for A, C and E, respectively.

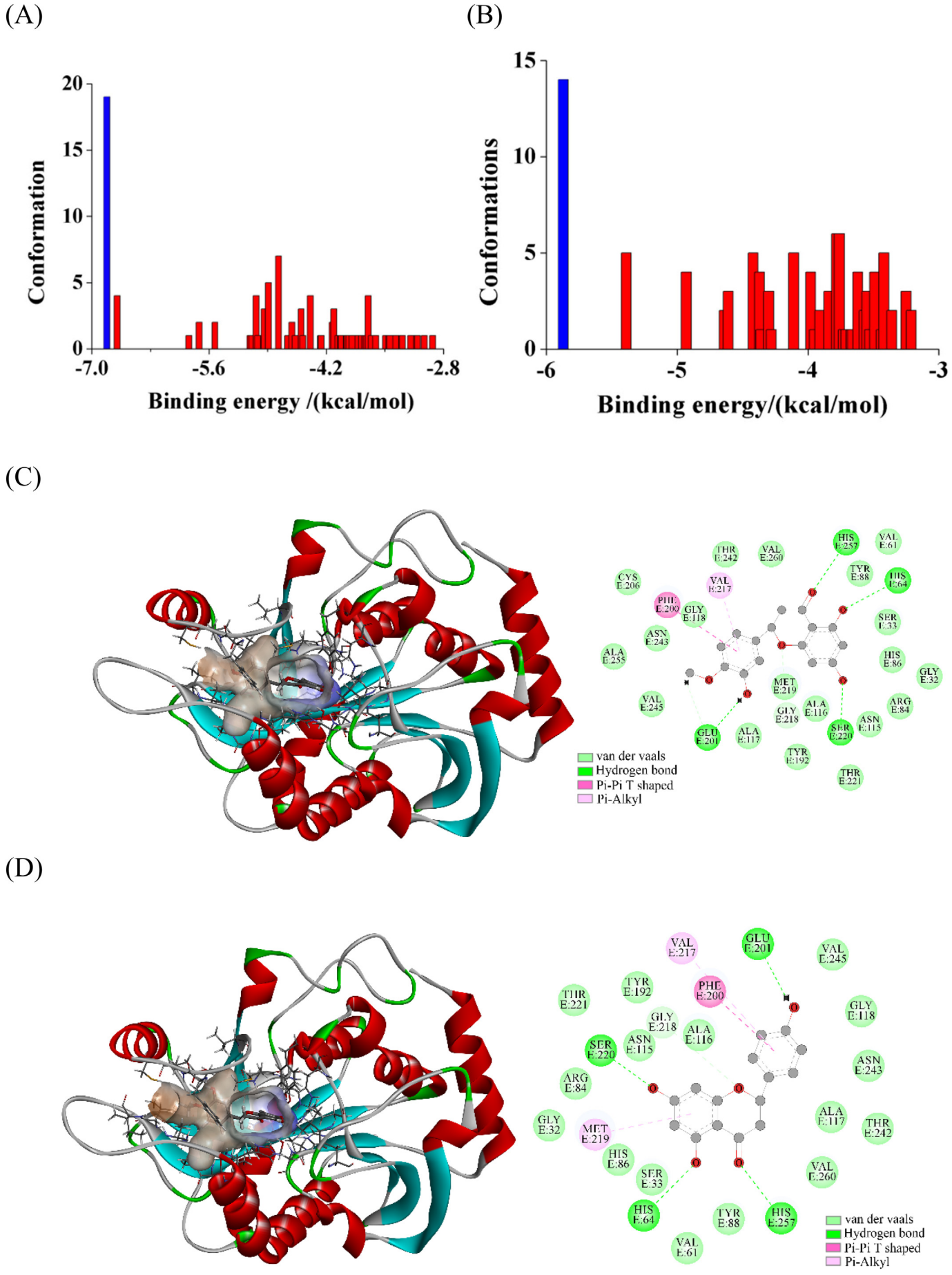

Fig. 8. Cluster analysis of the AutoDock docking runs of NAR (A) and HES (B) with hPNP; Three-dimensional (3D) and two-dimensional (2D) interaction patterns of hPNP with NAR (C) and HES (D) were generated using Discovery Studio Visualizer v4.0.

4. Conclusions

hPNP is one of the most important targets for therapy of T-cell malignancies, therefore finding significant inhibitors, especially from natural compounds is of importance. In the work, the inhibitory effects of two citrus flavonoids including NAR and HES on hPNP and interactions between them were investigated by a combination of differential experimental and computational methods. The results revealed that both NAR and HES could bind directly into the active cavity, and in this process induce the alterations in the microenvironment, secondary structure and morphology of hPNP, which resulted in the reduced catalytic activity and fluorescence quenching of hPNP. All these experimental results and theoretical data have provided some information for the interactions between NAR and HES and hPNP, and it would be valuable for understand the inhibitory mechanism of flavonoid compounds on hPNP, and search for other natural PNP inhibitors.

Declaration of competing interest

The authors hereby declare that there is no conflict of interest.

Acknowledgments

This research was supported by the National Natural Science Foundation of China (21706213) and Scientific Research Staring Foundation from the Northwest University, China. Financial support from the Chinese Postdoctoral Science Foundation (2016M602853) is also gratefully acknowledged.

References

[1] P. Giuliani, M. Zuccarini, S. Buccella, M. Rossini, I. D'Alimonte, R. Ciccarelli, M. Marzo, A. Marzo, P. Di Iorio, F. Caciagli, Development of a new HPLC method using fluorescence detection without derivatization for determining purine nucleoside phosphorylase activity in human plasma, J. Chromatogr. B 1009 (2016) 114–121.
[2] Q.H. Wen, L.H. Wang, X.A. Zeng, D.B. Niu, M.S. Wang, Hydroxyl-related differences for three dietary flavonoids as inhibitors of human purine nucleoside phosphorylase, Int. J. Biol. Macromol. 118 (2018) 588–598.
[3] M. Camici, V. Micheli, P.L. Ipata, M.G. Tozzi, Pediatric neurological syndromes and inborn errors of purine metabolism, Neurochem. Int. 56 (2010) 367–378.
[4] S. Kojima, T. Chiyomaru, K. Kawakami, H. Yoshino, H. Enokida, N. Nohata, M. Fuse, T. Ichikawa, Y. Naya, M. Nakagawa, Tumour suppressors miR-1 and miR-133a target the oncogenic function of purine nucleoside phosphorylase (PNP) in prostate cancer, Br. J. Cancer 106 (2012) 405–413.
[5] O. Sanfilippo, M. Camici, M.G. Tozzi, M. Turriani, A. Faranda, P. Ipata, R. Silvestrini, Relationship between the levels of purine salvage pathway enzymes and clinical/biological aggressiveness of human colon carcinoma, Cancer Biochem. Biophys. 14 (1994) 57–66.
[6] F. Ravandi, V. Gandhi, Novel purine nucleoside analogues for T-cell-lineage acute lymphoblastic leukaemia and lymphoma, Expert Opin. Investig. Drugs 15 (2006) 1601–1613.
[7] M.S. Castilho, M.P. Postigo, C.B. de Paula, C.A. Montanari, G. Oliva, A.D. Andricopulo, Two-and three-dimensional quantitative structure–activity relationships for a series of purine nucleoside phosphorylase inhibitors, Bioorg. Med. Chem. 14 (2006) 516–527.
[8] S. Das, P. Ghosh, S. Koley, A.S. Roy, Binding of naringin and naringenin with hen egg white lysozyme: a spectroscopic investigation and molecular docking study, Spectrochim. Acta A 192 (2018) 211–221.
[9] L. Chen, H. Teng, Z. Jia, M. Battino, A. Miron, Z. Yu, H. Cao, J. Xiao, Intracellular signaling pathways of inflammation modulated by dietary flavonoids: the most recent evidence, Crit. Rev. Food Sci. Nutr. 58 (2018) 2908–2924.
[10] J. Xiao, Dietary flavonoid aglycones and their glycosides: which show better biological significance? Crit. Rev. Food Sci. Nutr. 57 (2017) 1874–1905.
[11] D.H. Priscilla, D. Roy, A. Suresh, V. Kumar, K. Thirumurugan, Naringenin inhibits α-glucosidase activity: a promising strategy for the regulation of postprandial hyperglycemia in high fat diet fed streptozotocin induced diabetic rats, Chem. Biol. Interact. 210 (2014) 77–85.
[12] L. Quintieri, S. Bortolozzo, S. Stragliotto, S. Moro, M. Pavanetto, A. Nassi, P. Palatini, M. Floreani, Flavonoids diosmetin and hesperetin are potent inhibitors of cytochrome P450 2C9-mediated drug metabolism in vitro, Drug Metab. Pharmacokinet. 25 (2010) 466–476.
[13] B.B. Chandrika, M. Steephan, T.S. Kumar, A. Sabu, M. Haridas, Hesperetin and naringenin sensitize HER2 positive cancer cells to death by serving as HER2 tyrosine kinase inhibitors, Life Sci. 160 (2016) 47–56.
[14] S. Shahraki, H.S. Delarami, M. Saeidifar, Catalase inhibition by two Schiff base derivatives. Kinetics, thermodynamic and molecular docking studies, J. Mol. Liq. 287 (2019), 111003.
[15] R.M. Hjelm, K.E. Garcia, S. Babanova, K. Artyushkova, I. Matanovic, S. Banta, P. Atanassov, Functional interfaces for biomimetic energy harvesting: CNTs-DNA matrix for enzyme assembly, Biochim. Biophys. Acta Bioenerg. 1857 (2016) 612–620.
[16] Y. Wang, G. Zhang, J. Pan, D. Gong, Novel insights into the inhibitory mechanism of kaempferol on xanthine oxidase, J. Agric. Food Chem. 63 (2015) 526–534.
[17] M. Fan, H. Ding, G. Zhang, X. Hu, D. Gong, Relationships of dietary flavonoid structure with its tyrosinase inhibitory activity and affinity, LWT Food Sci. Technol. 107 (2019) 25–34.
[18] X. Wu, M. Hu, X. Hu, H. Ding, D. Gong, G. Zhang, Inhibitory mechanism of epicatechin gallate on α-amylase and α-glucosidase and its combinational effect with acarbose or epigallocatechin gallate, J. Mol. Liq. 290 (2019), 111202.
[19] A. Cornish-Bowden, R. Eisenthal, Statistical considerations in the estimation of enzyme kinetic parameters by the direct linear plot and other methods, Biochem. J. 139 (1974) 721–730.
[20] R. Yekta, G. Dehghan, S. Rashtbari, R. Ghadari, A.A. Moosavi-Movahedi, The inhibitory effect of farnesiferol C against catalase; kinetics, interaction mechanism and molecular docking simulation, Int. J. Biol. Macromol. 113 (2018) 1258–1265.
[21] D. Kalita, D.G. Holm, D.V. LaBarbera, J.M. Petrash, S.S. Jayanty, Inhibition of α-glucosidase, α-amylase, and aldose reductase by potato polyphenolic compounds, PLoS One 13 (2018).
[22] H.J. Zeng, Y.P. Wang, R. Yang, J. You, L.B. Qu, Inhibitory effects of daidzein and genistein on trypsin: insights from spectroscopic and molecular docking studies, Int. J. Biol. Macromol. 89 (2016) 336–343.
[23] L.H. Wang, M.S. Wang, X.A. Zeng, D.M. Gong, Y.B. Huang, An in vitro investigation of the inhibitory mechanism of β-galactosidase by cinnamaldehyde alone and in combination with carvacrol and thymol, Biochim. Biophys. Acta, Gen. Subj. 1861 ((2017) 3189–3198.
[24] R. Wang, X. Hu, J. Pan, G. Zhang, D. Gong, Interaction of isoeugenol with calf thymus DNA and its protective effect on DNA oxidative damage, J. Mol. Liq. 282 (2019) 356–365.
[25] X. Peng, G. Zhang, Y. Liao, D. Gong, Inhibitory kinetics and mechanism of kaempferol on α-glucosidase, Food Chem. 190 (2016) 207–215.
[26] W. Wang, N. Gan, Q. Sun, D. Wu, R. Gan, M. Zhang, P. Tang, H. Li, Study on the interaction of ertugliflozin with human serum albumin in vitro by multispectroscopic methods, molecular docking, and molecular dynamics simulation, Spectrochim. Acta A 219 (2019) 83–90.
[27] H. Yang, G. Hou, L. Zhang, L. Ju, C. Liu, Exploring the effect of bisphenol S on sludge hydrolysis and mechanism of the interaction between bisphenol S and α-amylase through spectrophotometric methods, J. Photochem. Photobiol. B 167 (2017) 128–135.
[28] M.Z. Kabir, Z. Benbekhti, N.F.W. Ridzwan, R. Merrouche, N. Bouras, S.B. Mohamad, S. Tayyab, Biophysical and in silico investigations of the molecular association between a potent RNA polymerase inhibitor, thiolutin and human serum albumin, J. Mol. Liq. 303 (2020) 1–11, https://doi.org/10.1016/j.molliq.2020.112648.
[29] S. Tayyab, M.M. Izzudin, M.Z. Kabir, S.R. Feroz, W.-V. Tee, S.B. Mohamad, Z. Alias, Binding of an anticancer drug, axitinib to human serum albumin: fluorescence quenching and molecular docking study, J. Photochem. Photobiol. B 162 (2016) 386–394.
[30] J.D. Stoeckler, R.P. Agarwal, K.C. Agarwal, K. Schmid, R.E. Parks Jr., Purine nucleoside phosphorylase from human erythrocytes: physicochemical properties of the crystalline enzyme, Biochemistry 17 (1978) 278–283.
[31] S. Lin, G. Zhang, Y. Liao, D. Gong, The inhibitory kinetics and mechanism of dietary vitamins D3 and B2 on xanthine oxidase, Food Funct. 7 (2016) 2849–2861.
[32] S. Farhadian, B. Shareghi, S. Asgharzadeh, M. Rajabi, H. Asadi, Structural characterization of α-chymotrypsin after binding to curcumin: spectroscopic and computational analysis of their binding mechanism, J. Mol. Liq. 289 (2019), 111111.
[33] C.P. Sun, J.K. Yan, J. Yi, X.Y. Zhang, Z.L. Yu, X.K. Huo, J.H. Liang, J. Ning, L. Feng, C. Wang, The study of inhibitory effect of natural flavonoids toward β-glucuronidase and interaction of flavonoids with β-glucuronidase, Int. J. Biol. Macromol. 143 (2020) 349–358.
[34] Z. Xiong, W. Liu, L. Zhou, L. Zou, J. Chen, Mushroom (Agaricus bisporus) polyphenoloxidase inhibited by apigenin: multi-spectroscopic analyses and computational docking simulation, Food Chem. 203 (2016) 430–439.
[35] Y. Zheng, W. Yang, W. Sun, S. Chen, D. Liu, X. Kong, J. Tian, X. Ye, Inhibition of porcine pancreatic α-amylase activity by chlorogenic acid, J. Funct. Foods 64 (2020), 103587.
[36] Z. Chen, Y. Chen, Z. Xue, X. Gao, Y. Jia, Y. Wang, Y. Lu, J. Zhang, M. Zhang, H. Chen, Insight into the inactivation mechanism of soybean Bowman-Birk trypsin inhibitor (BBTI) induced by epigallocatechin gallate and epigallocatechin: fluorescence, thermodynamics and docking studies, Food Chem. 303 (2020), 125380.